Crosstalk and error analysis of fat layer on continuous wave near-infrared spectroscopy measurements

Ömer Şayli
E. Burteçin Aksel
Ata Akın
Boğaziçi University,
Institute of Biomedical Engineering
Bebek, İstanbul, 34342, Turkey

Abstract. Accurate estimation of concentration changes in muscles by continuous wave near-IR spectroscopy for muscle measurements suffers from underestimation and crosstalk problems due to the presence of superficial skin and fat layers. Underestimation error is basically caused by a homogeneous medium assumption in the calculations leading to the partial volume effect. The homogeneous medium assumption and wavelength dependence of mean partial path length in the muscle layer cause the crosstalk. We investigate underestimation errors and crosstalk by Monte Carlo simulations with a three layered (skin-fat-muscle) tissue model for a two-wavelength system where the choice of first wavelength is in the 675- to 775-nm range and the second wavelength is in the 825- to 900-nm range. Means of absolute underestimation errors and crosstalk over the considered wavelength pairs are found to be higher for greater fat thicknesses. Estimation errors of concentration changes for Hb and HbO_2 are calculated to be close for an ischemia type protocol where both Hb and HbO_2 are assumed to have equal magnitude but opposite concentration changes. The minimum estimation errors are found for the 700/825- and 725/825-nm pairs for this protocol. © *2008 Society of Photo-Optical Instrumentation Engineers.* [DOI: 10.1117/1.3028008]

1 Introduction

Near infrared spectroscopy (NIRS) is increasingly used as an optical noninvasive method to monitor the changes in tissue oxygenation in brain,[1–3] breast,[4] and particularly in muscle tissues.[5–7] Continuous wave near-infrared spectroscopy (cw-NIRS) is based on a steady state technique where the changes in the detected light intensities at multiple wavelengths are converted to concentration changes of oxygenation sensitive chromophores. Typically, cw-NIRS is used in muscle physiology studies to calculate oxygen consumption and blood flow values. Spatially resolved spectroscopy[8] along with frequency and time domain techniques are other NIRS methods[9,10] that have the capability of quantifying absolute concentrations.

NIRS techniques suffer inaccuracies for the heterogonous tissue structures when the homogeneous medium assumption is made for the sake of simplicity.[11,12] In fact, there are solutions based on complex layered models[11–20] for NIRS. The degree of inaccuracy because of the homogeneous medium assumption depends on the region of interest, geometry, optical coefficients of the structures in the tissue, source-detector distance, and the choice of NIRS technique.[11,12,14,21–27] Hence, the estimated parameter (i.e., absorption coefficient change) could be related to a layer's (or to combination of layers)

property, or it may not be related to any property of any one of those layers at all.[12,14,28]

Muscle tissue has superficial skin and fat layers. A Fat layer has varying thicknesses between subjects and has a lower absorption coefficient than the underlying muscle layer, masking the muscle's optical parameters, hence making it difficult to determine the optical coefficients and quantify concentration changes in the lower muscle layer. It has been shown experimentally that adipose tissue causes sensitivity and linearity problems,[25,29–35] underestimation of oxygen consumption[36] in muscle cw-NIRS measurements in which modified Beer-Lambert law (MBLL) with a homogeneous medium assumption is used. These problems are mainly related to the so-called partial volume effect, which refers to the fact that hemodynamic changes occur in a volume smaller than that assumed by homogeneous medium assumption.[23,24,37]

Crosstalk in NIRS measurements refers to the measurement of chromophore concentration change although no real change happens for that chromophore but for other chromophores' concentrations.[23,24,38–41] This is caused again by the homogeneous medium assumption with the use of mean optical path length instead of wavelength-dependent partial optical path length in the tissue layer of interest where the concentration changes occur (i.e., muscle or gray matter in the

Address all correspondence to: Ata Akın. Tel: +90-212-359-74-88; Fax: +90-212-257-50-30; E-mail: ata.akin@boun.edu.tr.

brain). There are detailed studies on the analysis of the crosstalk effect for brain measurements, while as we know, there is only one study of Iwasaka and Okada[42] on the crosstalk effect for muscle measurements, where the analysis was done for a fixed fat thickness of 4 mm.

The effect of adipose tissue layer on cw-NIRS measurements with the homogeneous medium assumption using MBLL is investigated in our study by Monte Carlo simulations for a two-wavelength system. Simulations were performed for a homogeneous layered skin-fat-muscle heterogeneous tissue model with varying fat thickness up to 15 mm. The wavelengths are in 675- to 775-nm range for the first wavelength and in 825- to 900-nm range for the second wavelength, and in total 24 wavelength pairs were used. For the considered wavelengths and fat thicknesses, mean partial path lengths in the three layers and detected light intensities were found. An error analysis for estimated concentration changes was analyzed by partitioning the error into an underestimation term for a real change in muscle layer and a crosstalk term, where the aims are the investigation of the fat layer thickness effect and a search for wavelength pairs that result in low errors. An error analysis for a particular measurement protocol of vascular occlusion is also discussed.

2 Theory

2.1 Homogeneous Medium Assumption

The cw-NIRS technique relies on the MBLL to convert detected light intensity changes into concentration changes of chromophores. For a single light absorber in a homogeneous medium, light attenuation is given by[1]

$$OD^\lambda = \ln(I_o/I) = \epsilon^\lambda c \, DPF^\lambda r + G^\lambda, \qquad (1)$$

where superscript λ indicates a particular wavelength, OD^λ is optical density, I_o is the intensity of the light sent into the tissue, I is the intensity of the detected light, ϵ^λ and c are the specific absorption coefficient (OD/cm mM^{-1}) and concentration (millimolar) of the chromophore in the medium, respectively; r (in centimeters) is the minimal geometric distance between light source and detector, and DPF^λ is the differential path length factor. DPF^λ equals mean optical path length of the photons ($\langle L^\lambda \rangle$) divided by r. Also, the G^λ factor is due to medium geometry and light scattering. The absorption coefficient of the medium μ_a^λ is equal to $\epsilon^\lambda c$. The change in the logarithm of detected light intensity (ΔOD^λ) is proportional to concentration change of the absorber (Δc, assumed to be homogeneous and small), given by $\Delta OD^\lambda = \epsilon^\lambda \Delta c \langle L^\lambda \rangle$, a differential form of the MBLL. Here it is assumed that G^λ and $\langle L^\lambda \rangle$ do not change during measurement. This formula and Eq. (1) of MBLL neglect the variation of $\langle L^\lambda \rangle$ with μ_a^λ. In fact, $\langle L^\lambda \rangle$ should be replaced by its mean value computed over the range of absorption coefficient[43] from 0 to μ_a^λ. Nevertheless, MBLL formulation can still be used to determine concentration changes for small absorption changes for which $\langle L^\lambda \rangle$ remains nearly constant.[22,43,44] Light scattering change is another issue.[44]

For tissues where the main light absorbers are Hb and HbO$_2$,

$$\Delta OD^\lambda = (\epsilon_{Hb}^\lambda \Delta[Hb] + \epsilon_{HbO_2}^\lambda \Delta[HbO_2]) DPF^\lambda r, \qquad (2)$$

assuming a homogeneous tissue medium. For a two-wavelength cw-NIRS system, concentration changes are estimated using MBLL as follows;

$$\Delta[Hb]_{MBLL} = \frac{(\epsilon_{HbO_2}^{\lambda_2} \Delta OD^{\lambda_1}/(DPF)^{\lambda_1}) - (\epsilon_{HbO_2}^{\lambda_1} \Delta OD^{\lambda_2}/(DPF)^{\lambda_2})}{r(\epsilon_{HbO_2}^{\lambda_2} \epsilon_{Hb}^{\lambda_1} - \epsilon_{HbO_2}^{\lambda_1} \epsilon_{Hb}^{\lambda_2})}, \qquad (3)$$

$$\Delta[HbO_2]_{MBLL} = \frac{(\epsilon_{Hb}^{\lambda_1} \Delta OD^{\lambda_2}/(DPF)^{\lambda_2}) - (\epsilon_{Hb}^{\lambda_2} \Delta OD^{\lambda_1}/(DPF)^{\lambda_1})}{r(\epsilon_{HbO_2}^{\lambda_2} \epsilon_{Hb}^{\lambda_1} - \epsilon_{HbO_2}^{\lambda_1} \epsilon_{Hb}^{\lambda_2})}. \qquad (4)$$

The MBLL subscript indicates that estimated concentration changes are found using a homogeneous-medium-assumption-based MBLL formulation. In general, a wavelength-independent DPF is used in the MBLL calculations.

Note that for the considered muscle measurements, [Hb] ([HbO$_2$]) refers to combined concentrations of deoxyhemoglobin and deoxymyoglobin (oxyhemoglobin and oxymyoglobin) since hemoglobin and myoglobin have very similar absorption spectra.[45]

2.2 Underestimation Error and Crosstalk

For muscle cw-NIRS measurements, a more realistic tissue model should contain skin, fat, and muscle tissue layers. Measured optical density change can be written as[22]

$$\Delta OD^\lambda = \Delta\mu_{a,s}\langle L_s^\lambda \rangle + \Delta\mu_{a,f}\langle L_f^\lambda \rangle + \Delta\mu_{a,m}\langle L_m^\lambda \rangle, \qquad (5)$$

where $\langle L_s^\lambda \rangle$, $\langle L_f^\lambda \rangle$, and $\langle L_m^\lambda \rangle$ are the mean partial path lengths of the detected light and $\Delta\mu_{a,s}$, $\Delta\mu_{a,f}$, $\Delta\mu_{a,m}$ are the homogeneous absorption changes in the skin, fat, and muscle layers, respectively. Assuming that the concentration changes mainly occur in the muscle layer, Eq. (5) becomes

$$\Delta OD^\lambda \cong (\epsilon_{Hb}^\lambda \Delta[Hb]_m + \epsilon_{HbO_2}^\lambda \Delta[HbO_2]_m)\langle L_m^\lambda \rangle, \qquad (6)$$

where $\Delta[Hb]_m$ and $\Delta[HbO_2]_m$ are the real concentration changes in the muscle layer. Substituting Eq. (6) for measured optical density changes ΔOD^λ in Eqs. (3) and (4), the estimated concentration changes using MBLL can be written as[24]

$$\Delta[X]_{MBLL} = U_X \Delta[X]_m + C_X \Delta[O]_m \qquad (7)$$

where X represents the chromophore being either Hb or HbO$_2$ and O represents the other chromophore, HbO$_2$ or Hb, $\Delta[X]_m$ and $\Delta[O]_m$ are the real concentration changes in the muscle layer, U_X corresponds to the underestimation of $\Delta[X]_m$, and C_X represents crosstalk from other chromophore $\Delta[O]_m$ to estimated $\Delta[X]_{MBLL}$, given by

$$U_{Hb} = \frac{\epsilon_{Hb}^{\lambda_1} \epsilon_{HbO_2}^{\lambda_2} l^{\lambda_1} - \epsilon_{Hb}^{\lambda_2} \epsilon_{HbO_2}^{\lambda_1} l^{\lambda_2}}{\epsilon_{Hb}^{\lambda_1} \epsilon_{HbO_2}^{\lambda_2} - \epsilon_{Hb}^{\lambda_2} \epsilon_{HbO_2}^{\lambda_1}}, \qquad (8)$$

$$U_{HbO_2} = \frac{\epsilon_{Hb}^{\lambda_1} \epsilon_{HbO_2}^{\lambda_2} l^{\lambda_2} - \epsilon_{Hb}^{\lambda_2} \epsilon_{HbO_2}^{\lambda_1} l^{\lambda_1}}{\epsilon_{Hb}^{\lambda_1} \epsilon_{HbO_2}^{\lambda_2} - \epsilon_{Hb}^{\lambda_2} \epsilon_{HbO_2}^{\lambda_1}}, \qquad (9)$$

$$C_{\text{Hb}} = \frac{\epsilon_{\text{HbO}_2}^{\lambda_1} \epsilon_{\text{HbO}_2}^{\lambda_2}}{\epsilon_{\text{Hb}}^{\lambda_1} \epsilon_{\text{HbO}_2}^{\lambda_2} - \epsilon_{\text{Hb}}^{\lambda_2} \epsilon_{\text{HbO}_2}^{\lambda_1}} (l^{\lambda_1} - l^{\lambda_2}), \qquad (10)$$

$$C_{\text{HbO}_2} = \frac{\epsilon_{\text{Hb}}^{\lambda_1} \epsilon_{\text{Hb}}^{\lambda_2}}{\epsilon_{\text{Hb}}^{\lambda_1} \epsilon_{\text{HbO}_2}^{\lambda_2} - \epsilon_{\text{Hb}}^{\lambda_2} \epsilon_{\text{HbO}_2}^{\lambda_1}} (l^{\lambda_2} - l^{\lambda_1}), \qquad (11)$$

where $l^{\lambda} = \langle L_m^{\lambda} \rangle / (\text{DPF}^{\lambda} \times r)$. For a theoretical case of zero skin and fat thicknesses, mean optical path length $\langle L^{\lambda} \rangle$ will be equal to $\langle L_m^{\lambda} \rangle$, which can be accurately measured by time or frequency domain NIRS systems. Hence, this value can be used to find DPF^{λ} factor, i.e., $\text{DPF}^{\lambda_1} = \langle L_m^{\lambda_1} \rangle / r$ and $\text{DPF}^{\lambda_2} = \langle L_m^{\lambda_2} \rangle / r$. Underestimation terms U_{Hb} and U_{HbO_2} then have ideal values of 1 because both l^{λ_1} and l^{λ_2} are equal to one. Crosstalk terms C_{Hb} and C_{HbO_2} are null since l^{λ_1} and l^{λ_2} would be one, making their difference zero. However, in practice, there are these superficial layers and measurement of $\langle L_m^{\lambda} \rangle$ alone is not possible. Magnitudes of crosstalk terms C_{Hb} and C_{HbO_2} are proportional to the difference of $l^{\lambda_1} - l^{\lambda_2}$. For the use of wavelength independent DPF, C_{Hb} and C_{HbO_2} are zero when $\langle L_m^{\lambda_1} \rangle = \langle L_m^{\lambda_2} \rangle$. Hence, one of the ways to minimize crosstalk is to utilize a wavelength pair for which partial optical path length in the layer of interest (i.e., gray matter in the brain) are equal.[46] In summary, the magnitude of underestimation and crosstalk terms depend on the wavelength dependence of specific absorption coefficients, choice of DPF^{λ} factors, which are used instead of unavailable $\langle L_m^{\lambda} \rangle / r$.

A common definition for crosstalk is the ratio of the estimated concentration change of the chromophore X for which no change happens to the estimated concentration change of the chromophore O for which real change is induced,[40,46] denoted as $C_{\text{O} \rightarrow \text{X}}$. According to this definition and previous formulation, $C_{\text{HbO}_2 \rightarrow \text{Hb}}$ and $C_{\text{Hb} \rightarrow \text{HbO}_2}$ are

$$C_{\text{HbO}_2 \rightarrow \text{Hb}}(\%) = 100 \times C_{\text{Hb}} / U_{\text{HbO}_2}, \qquad (12a)$$

$$C_{\text{Hb} \rightarrow \text{HbO}_2}(\%) = 100 \times C_{\text{HbO}_2} / U_{\text{Hb}}. \qquad (12b)$$

In this study, underestimation error (in percent) refers to $(1 - U_{\text{X}}) \times 100$ for the corresponding U_{X} factor. For the crosstalk, formulas given in Eqs. (12a) and (12b) are used. The estimation error for the concentration change of chromophore X in the muscle layer using MBLL is given by

$$E_{\text{MBLL}} = 100 \times (\Delta[\text{X}]_{\text{MBLL}} - \Delta[\text{X}]_m) / \Delta[\text{X}]_m \% . \quad (13)$$

In this analysis, small concentration changes are assumed so that partial path length in the muscle layer remains constant such that calculated U_{X} and C_{X} terms along with underestimation and crosstalk errors are constant values for specific wavelength pair and fat thickness.

3 Methods

3.1 Tissue Model

For the simulations, three homogeneously layered skin-fat-muscle heterogeneous model is used. Skin thickness is taken to be 1.4 mm and muscle thickness is infinite. Reduced scattering coefficients of the three tissues and absorption coeffi-

cients of skin and adipose tissues are taken from Simpson et al.[47] For the muscle tissue, the absorption coefficient is calculated with the equation

$$\mu_{a,m}^{\lambda} = \mu_{a,w}^{\lambda} V_w + [t\text{Hb}][\epsilon_{\text{HbO}_2}^{\lambda} \text{StO}_2 + \epsilon_{\text{Hb}}^{\lambda}(1 - \text{StO}_2)] + \mu_{a,b}, \qquad (14)$$

where $\mu_{a,w}^{\lambda}$ is the water absorption coefficient, V_w is water fraction of muscle tissue, $[t\text{Hb}]$ is total hemoglobin concentration, StO_2 is oxygen saturation, and $\mu_{a,b}$ is background absorption. In the calculation, V_w, StO_2, and $[t\text{Hb}]$ are taken as 70%, 70%, and 100 μM, respectively, as typical values.[48,49] The $\mu_{a,w}^{\lambda}$ values are taken from the study of Hollis.[50] The background absorption coefficient of muscle tissue $\mu_{a,b}$ is taken as 0.072 cm^{-1} so that the calculated $\mu_{a,m}^{798 \text{ nm}}$ equals the experimentally found *in vitro* value of Simpson et al.[47] since absorption at this isobestic point is unaffected by the oxygen saturation of the hemoglobin. Table 1 lists the absorption and reduced scattering coefficients of the three layers used in the simulations.

3.2 Monte Carlo Simulations

In a Monte Carlo simulation of photon propagation in biological tissues, a stochastic model was constructed in which rules of photon propagation were modeled in the form of probability distributions.[51] In the simulation, photons were launched with initial direction along z axis (the axis perpendicular to tissue layers) from a point source. For a photon traveling in layer i, which has absorption coefficient $\mu_{a,i}$, scattering coefficient $\mu_{s,i}$, and reduced scattering coefficient $\mu_{s,i}'$ [which is equal to $(1-g)\mu_{s,i}$, where g is the mean cosine of the single scattering phase function and is called anisotropy factor], successive scattering distances are selected using a random variable $l = -\ln(R)/\mu_{s,i}'$, with R having a uniform distribution over (0,1]. The remaining scattering length Δl_i for photons crossing tissue boundary from medium i to medium j is recalculated by $\Delta l_j = \Delta l_i \mu_{s,i}' / \mu_{s,j}'$. Isotropic scattering is utilized using principle of similarity.[52] Scatter azimuthal angle was uniformly distributed over the interval $[0, 2\pi)$. Fresnel formulas are used for reflection or transmission at the boundaries.[51]

Total distance traveled in layer i by a photon (L_i) was found by summing scattering lengths taken in this layer. Photon propagation was continued until it escapes the medium or travels 220 cm in length (10 ns). For those reaching the surface, exit (survival) weight (w) is calculated using Lambert-Beer law as $w = w_0 \exp[-\Sigma_i (L_i \mu_{a,i})]$, with w_0 accounting for reflections and refractions at the boundaries encountered by the particular photon when there are refractive index mismatches.[22] Because of the symmetry of the medium considered, photons reaching a ring (thickness is dr, distance from center of ring to the light source is r) were taken as the photons reaching the detector. The mean partial path length in medium i ($\langle L_i \rangle$) for the detected photons was found using the formula $\langle L_i \rangle = \Sigma_{j=1}^{N} L_{i,j} w_j / (\Sigma_{j=1}^{N} w_j)$, where $L_{i,j}$ is the total path length taken in medium i by detected photon j with weight w_j, and N is total number of detected photons. Refractive indices of air and tissue layers were taken to be 1 and 1.4, respectively.[53] Each simulation was performed using 5×10^7 photons and the dr thickness is taken to be 0.5 cm.

Table 1 Optical properties of the skin, fat and muscle tissue layers used in the simulations (for log base e).

λ (nm)	μ_a (cm^{-1})			μ_s' (cm^{-1})		
	Skin	Fat	Muscle	Skin	Fat	Muscle
675	0.232	0.097	0.321	24.81	12.24	8.53
700	0.191	0.089	0.254	23.17	12.03	8.08
725	0.172	0.089	0.243	21.99	11.87	7.89
750	0.165	0.092	0.288	20.97	11.67	7.69
760	0.159	0.093	0.306	20.53	11.61	7.50
775	0.146	0.087	0.291	19.91	11.50	7.21
800	0.127	0.083	0.284	19.07	11.36	6.99
825	0.121	0.085	0.309	18.24	11.12	6.78
850	0.122	0.086	0.343	17.57	11.09	6.60
875	0.122	0.091	0.368	16.98	10.97	6.43
900	0.134	0.125	0.393	16.30	10.88	6.32

4 Results

4.1 Path Lengths and Detected Light Intensity

We performed Monte Carlo simulations to calculate the mean partial path lengths for the 11 distinct wavelengths given in Table 1. Note that $\langle L_{i,r,h_f}^\lambda \rangle$ represents the mean partial path length in layer i (s, f, or m for skin, fat, and muscle, respectively, as used in Sec. 2.2), for a source-detector distance r (in centimeters), at fat thickness h_f (in millimeters) and wavelength λ. Also $\langle L_{i,r,h_f} \rangle$ denotes the mean ± standard deviation of the mean partial path length in layer i computed over all wavelengths.

The term $\langle L_m^\lambda \rangle$ is the most important variable affecting the underestimation error and crosstalk, as shown in Fig. 1. The value of $\langle L_{m,3.0,h_f}^\lambda \rangle$ decreased linearly with a higher slope for $0 \leqslant h_f \leqslant 7$ mm, while the slope decreased for $h_f > 7$ mm. The value of $\langle L_{m,3.0,0} \rangle$ is 11.5 ± 1.20 cm and that of $\langle L_{m,3.0,7} \rangle$ is 2.35 ± 0.43 cm. Above 10 mm of fat thickness, $\langle L_{m,3.0,h_f}^\lambda \rangle$ decreased much more slowly but eventually approached null, where $\langle L_{m,3.0,15} \rangle = 0.20 \pm 0.04$ cm. It was possible to infer a considerable wavelength-dependent variability in $\langle L_{m,3.0,h_f}^\lambda \rangle$. The value of $\langle L_{m,3.0,h_f}^\lambda \rangle$ was found to increase from 675 to 725 nm, while it had a decreasing trend from the 725- to 900-nm range. This finding can be explained by the wavelength dependence of the optical properties of muscle and fat tissues given in Table 1. The coefficient of variation (CV = standard deviation/mean) of $\langle L_{m,3.0,h_f}^\lambda \rangle$ values over 11 wavelengths increased from 11% at $h_f = 0$ mm to 23% at $h_f = 15$ mm.

The value of $\langle L_{s,3.0,h_f}^\lambda \rangle$ was found to be the least varying mean partial path length with respect to h_f variation with val-

ues ranging from 1.78 to 2.39 cm having a maximum at around $h_f = 6$ to 7 mm for all considered wavelengths. In contrast to $\langle L_{m,r,h_f}^\lambda \rangle$, $\langle L_{f,r,h_f}^\lambda \rangle$ and mean path length increased with increasing h_f as expected. The value of $\langle L_{f,3.0,h_f} \rangle$ ranged from 1.84 ± 0.13 cm at a 1-mm fat thickness to 21.77 ± 1.24 cm at $h_f = 15$ mm, while the mean path length ranged from
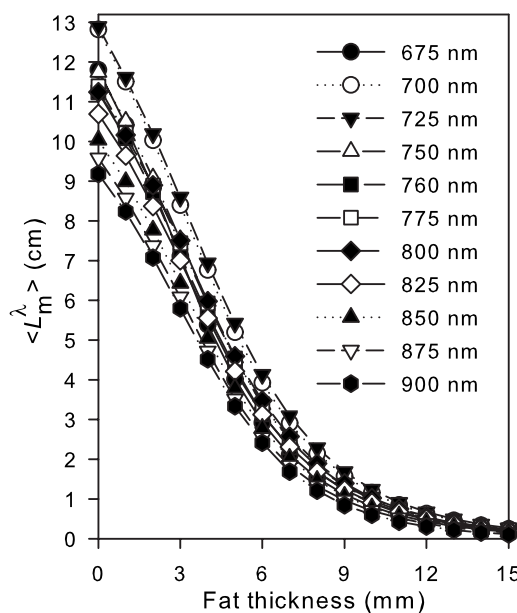
Fig. 1 Mean partial path length in the muscle layer for various wavelengths in the range 675 to 900 nm and fat thicknesses up to 15 mm estimated by Monte Carlo simulations ($r = 3.0$ cm).

13.03 ± 1.26 cm at $h_f = 0$ mm to 24.17 ± 1.30 cm at $h_f = 15$ mm. The mean path length had a decreasing trend with local peaks at either 700 or 725 nm and either 775 or 800 nm.

An increase in the fat layer thickness caused an increase in the detected light intensity. These increases in the detected light intensities for the 11 wavelengths expressed as mean $\pm$ standard deviation were 74 ± 28, 272 ± 97, and $537 \pm 184\%$ at $h_f = 4$, 8, and 15 mm, respectively, with respect to detected intensities at $h_f = 0$ mm ($r = 3.0$ cm).

With increase in source-detector distance, $\langle L_m^\lambda \rangle$ and mean path length increased, while detected light intensity decreased. In particular, $\langle L_{m,4.0,0} \rangle = 15.31 \pm 1.65$ cm, and $\langle L_{m,4.0,7} \rangle = 4.31 \pm 0.75$ cm.

4.2 Underestimation Error

Underestimation errors were calculated for a two-wavelength cw-NIRS system under varying fat thicknesses. The two wavelengths were chosen to fall before and after the isobestic point at around 800 nm. Hence, there were 24 wavelength pairs λ_1 / λ_2, where λ_1 is between 675 and 775 nm and λ_2 is between 825 and 900 nm. DPF was taken to be wavelength independent with a value of 4.37 found for $h_f = 0$ and $\lambda = 800$ nm. Underestimation error for the pair λ_1 / λ_2 is denoted by $E_{X,r,h_f}^{\lambda_1,\lambda_2}$, where the first subscript refers to the chromophore, the second and (if present) third subscripts refer to source-detector distance (in centimeters), and the h_f value (in millimeters), respectively. For the all considered λ_1 / λ_2 pairs, E_{X,r,h_f} showed mean $\pm$ standard deviation of the absolute values of the underestimation errors $E_{X,r,h_f}^{\lambda_1,\lambda_2}$.

Figures 2(a) and 2(b) show $E_{Hb,3.0,h_f}$ and $E_{HbO_2,3.0,h_f}$ along with minimum errors for $E_{Hb,3.0,h_f}^{\lambda_1,\lambda_2}$ and $E_{HbO_2,r,h_f}^{\lambda_1,\lambda_2}$. The 725/900-nm pair gives the minimum values for $E_{Hb,3.0,h_f}^{\lambda_1,\lambda_2}$ except at $h_f = 0$ mm, for which the 700/825-nm pair gives the minimum error. The 675/825-nm pair gives the minimum error for $E_{HbO_2,r,h_f}^{\lambda_1,\lambda_2}$ from $h_f = 0$ mm up to and including 10 mm, and at higher h_f values, the 760/825-nm pair is the minimum error producing pair. Both the errors $E_{Hb,3.0,h_f}$ and $E_{HbO_2,3.0,h_f}$ exhibited a steep increase in the fat thickness range < 5 mm and a decreasing slope beyond this value. Interestingly, $E_{Hb,3.0,h_f}$ began at a lower value compared to $E_{HbO_2,3.0,h_f}$ but had a larger slope in this range. As expected, $E_{Hb,3.0,h_f}$ and $E_{HbO_2,3.0,h_f}$ approached a complete underestimation error (100%) at $h_f = 15$ mm. For the no-fat-thickness case, $E_{Hb,3.0,0}$ was $6.1 \pm 3.5\%$ and $E_{HbO_2,3.0,0}$ was $28.9 \pm 5.8\%$. The slopes of the least-squares fits to the absolute values of underestimation errors in $h_f = 0$ to 5 mm range were $11.5\%/$mm ($R^2 = 0.94$) for $|E_{Hb,3.0}^{\lambda_1,\lambda_2}|$ and $9.1\%/$mm ($R^2 = 0.91$) for $|E_{HbO_2,3.0}^{\lambda_1,\lambda_2}|$.

There is wavelength pair dependency in the underestimation errors. The value of $E_{Hb,3.0}^{\lambda_1,\lambda_2}$ decreased in magnitude for an increase in λ_2, while that of $E_{HbO_2,3.0}^{\lambda_1,\lambda_2}$ increased, for fixed λ_1 at a given h_f. This change of variation over λ_2 was higher for $E_{HbO_2,3.0}^{\lambda_1,\lambda_2}$. The variation of λ_1—for fixed λ_2 at a given h_f—led to a high range of change for $E_{Hb,3.0}^{\lambda_1,\lambda_2}$, where 700 and 725 nm lead to lower errors. Underestimation errors for $h_f = 2$ mm are given in Table 2 to show wavelength pair effect. The wave-
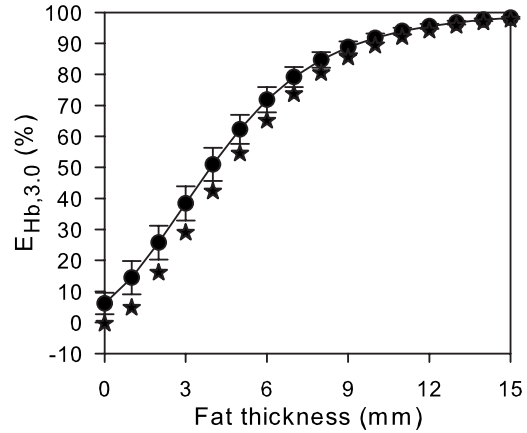
(a)
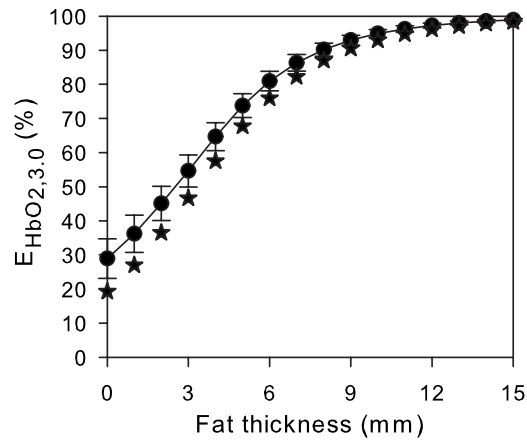
(b)

Fig. 2 Plots of (a) $E_{Hb,3.0}$ (%) and (b) $E_{HbO_2,3.0}$ (%), which are the mean$\pm$standard deviation of absolute respective underestimation errors computed over all considered λ_1 / λ_2 pairs for fat thicknesses up to 15 mm. Minimum individual errors for $E_{Hb,3.0,h_f}^{\lambda_1,\lambda_2}$ and $E_{HbO_2,3.0,h_f}^{\lambda_1,\lambda_2}$ are shown as stars.

length pair dependency of underestimation errors decreasd with h_f increase. CV values of absolute underestimation errors were 56.5% (20.0%) at $h_f = 0$ mm and 0.3% (0.4%) at $h_f = 15$ mm for $|E_{Hb,3.0}^{\lambda_1,\lambda_2}|$ ($|E_{HbO_2,3.0}^{\lambda_1,\lambda_2}|$) over the considered λ_1 / λ_2 pairs.

For longer source-detector distance of 4.0 cm, errors are lower. Here, $E_{Hb,4.0,0}$ and $E_{HbO_2,4.0,0}$ were 5.7 ± 2.3 and $26.7 \pm 5.7\%$, respectively. The slopes of the least-squares fits in the 0 to 5-mm fat thickness range are $9.9\%/$mm ($R^2 = 0.89$) for $|E_{Hb,4.0}^{\lambda_1,\lambda_2}|$ and $8.0\%/$mm ($R^2 = 0.88$) for $|E_{HbO_2,4.0}^{\lambda_1,\lambda_2}|$. Again above $h_f = 10$ mm, $E_{Hb,4.0}$ ($E_{HbO_2,4.0}$) became very high, with values above $87.3 \pm 2.3\%$ ($92.1 \pm 1.5\%$).

4.3 Crosstalk Analysis

Crosstalk was calculated using Eqs. (12a) and (12b) for the two-wavelength system represented by $C_{O \rightarrow X,r,(h_f)}^{\lambda_1,\lambda_2}$, where the superscripts refer to particular wavelength pair and first, second, and third (if present) subscripts represent crosstalk type, source-detector distance (in centimeters), and h_f value (millimeters), respectively. Crosstalk was computed for the same

Table 2 Underestimation errors $E_{Hb,3.0,2}^{\lambda_1,\lambda_2}$ (in percentages) and $E_{HbO_2,3.0,2}^{\lambda_1,\lambda_2}$ (in percentages) for the considered λ_1/λ_2 pairs.

	λ_1 (nm)	675	700	725	750	760	775
	λ_2 (nm)						
	825	32.4	21.6	18.0	28.7	32.4	29.2
$E_{Hb,3.0,2}^{\lambda_1,\lambda_2}$ (%)	850	32.0	21.2	17.4	27.6	31.1	26.9
	875	31.8	20.9	16.8	26.8	30.2	25.4
	900	31.6	20.5	16.1	26.0	29.4	23.9
	825	36.5	38.1	40.4	38.2	37.2	39.2
$E_{HbO_2,3.0,2}^{\lambda_1,\lambda_2}$ (%)	850	41.4	43.0	45.6	43.9	43.1	46.0
	875	44.7	46.4	49.2	47.7	47.0	50.5
	900	47.1	49.0	52.1	50.8	50.1	54.3

λ_1/λ_2 pairs in underestimation error computations. DPF was assumed to be taken as wavelength independent, for which case crosstalk defined by Eq. (12) resulted in DPF independence. Not that $C_{O \to X,r,(h_f)}$ represents mean $\pm$ standard deviation of absolute values of crosstalk $|C_{O \to X,r,(h_f)}^{\lambda_1,\lambda_2}|$ for the all λ_1/λ_2 pairs.

In general, $C_{HbO_2 \to Hb,3.0}^{\lambda_1,\lambda_2}$ had positive values, while $C_{Hb \to HbO_2,3.0}^{\lambda_1,\lambda_2}$ had negative values. The minimum-error-producing pairs for $C_{HbO_2 \to Hb,3.0}^{\lambda_1,\lambda_2}$ were the 675/825-nm pair at $h_f=0$ mm up to including 5 mm, the 760/825-nm pair at $h_f=6,7,$ and 9 mm; and the 675/850-nm pair at other h_f values. Also $C_{Hb \to HbO_2,3.0}^{\lambda_1,\lambda_2}$ had the minimum errors for the 760/825-nm pair at $h_f=0,1,2,4,5,6,7,8,9,$ and 10 mm, for the 675/825-nm pair at $h_f=3$ mm; for the 675/850-nm pair at $h_f=11,12,13,$ and 14 mm; and for the 750/825-nm pair at $h_f=15$ mm. The values $C_{HbO_2 \to Hb,3.0}$ (about 9.5%) and $C_{Hb \to HbO_2,3.0}$ (about 14.2%) were nearly constant in the $h_f=0$ to 3-mm range, as shown in Fig. 3 While in the $h_f=3$- to 14-mm $C_{HbO_2 \to Hb,3.0}$ increased up to $25.0 \pm 34.9\%$, $C_{Hb \to HbO_2,3.0}$ showed an increasing trend in the $h_f=3$- to 10-mm range, with $C_{Hb \to HbO_2,3.0,10}=20.3 \pm 10.2\%$. The slopes of the least-squares fits in these respective h_f ranges to the absolute crosstalk values were 1.4%/mm ($R^2=0.1$) for $|C_{HbO_2 \to Hb,3.0}^{\lambda_1,\lambda_2}|$ and 0.9%/mm ($R^2=0.1$) for $|C_{Hb \to HbO_2,3.0}^{\lambda_1,\lambda_2}|$.

In Table 3, crosstalk values are given for $h_f=-0$-, 5-, 10-, and 15-mm values for all wavelength pairs. Similar to the increase seen in the mean values the standard deviations of absolute crosstalk over considered wavelength pairs showed dramatic increases as the fat thickened. The $C_{HbO_2 \to Hb,3.0}^{\lambda_1,\lambda_2}$ had CV values of 64.9, 82.3, and 159.2% at h_f values of 0, 5, and 15 mm, respectively. The $C_{Hb \to HbO_2,3.0}^{\lambda_1,\lambda_2}$ had lower CV values of 31.0, 47.0, and 57.6% at $h_f=0$, 5, and 15 mm. However, $C_{Hb \to HbO_2,3.0}^{\lambda_1,\lambda_2}$ had higher magnitudes in general. Examining the results from Table 3, we can observe that both absolute values of crosstalk are less than 11% for pairs 675/825,
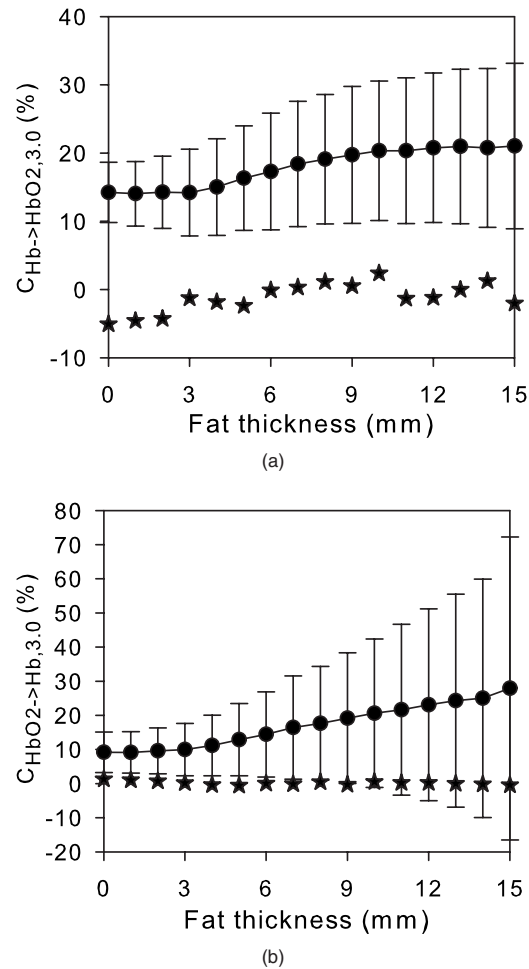
Fig. 3 Plots of (a) $C_{Hb \to HbO_2,3.0,h_f}$ (%) and (b) $C_{HbO_2 \to Hb,3.0,h_f}$ (%), which are the mean±standard deviation of absolute respective crosstalk computed over all considered λ_1/λ_2 pairs for fat thicknesses up to 15 mm. Minimum individual errors for $C_{Hb \to HbO_2,3.0,h_f}^{\lambda_1,\lambda_2}$ and $C_{HbO_2 \to Hb,3.0,h_f}^{\lambda_1,\lambda_2}$ are shown as stars.

Table 3 Crosstalk values $C_{\mathrm{Hb}\to\mathrm{HbO}_2,3.0,h_f}^{\lambda_1,\lambda_2}$ (in percentages) and $C_{\mathrm{HbO}_2\to\mathrm{Hb},3.0,h_f}^{\lambda_1,\lambda_2}$ (in percentages) for different λ_1/λ_2 pairs and $h_f=0$, 5, 10, and 15 mm.

Fat thickness	λ_1 (nm)	$C_{\mathrm{Hb}\to\mathrm{HbO}_2,3.0,h_f}^{\lambda_1,\lambda_2}$ (%)						$C_{\mathrm{HbO}_2\to\mathrm{Hb},3.0,h_f}^{\lambda_1,\lambda_2}$ (%)					
		675	700	725	750	760	775	675	700	725	750	760	775
	λ_2 (nm)												
0 mm	825	−7.8	−14.3	−16.2	−9.1	−5.1	−7.9	1.3	4.2	8.8	5.0	2.6	6.8
	850	−10.8	−16.2	−17.9	−12.3	−9.2	−12.1	2.2	5.7	11.9	8.4	6.0	13.3
	875	−13.1	−18.0	−19.7	−14.8	−12.1	−15.0	2.9	7.0	14.5	11.2	8.7	18.9
	900	−15.7	−20.6	−22.4	−17.8	−15.1	−18.5	3.6	8.3	17.4	14.2	11.6	25.3
5 mm	825	4.1	−16.3	−20.9	−7.6	−2.4	−9.1	−0.6	4.9	12.7	4.1	1.2	8.1
	850	−4.0	−20.0	−23.8	−14.1	−10.3	−16.3	0.7	7.7	18.8	9.9	6.8	20.3
	875	−8.7	−22.9	−26.4	−18.1	−14.9	−20.5	1.8	10.1	24.1	14.9	11.5	31.1
	900	−12.0	−25.7	−29.3	−21.4	−18.4	−24.3	2.6	11.9	28.8	19.1	15.4	41.3
10 mm	825	10.3	−18.2	−24.5	−5.9	2.4	−9.6	−1.3	5.7	16.2	3.0	−1.1	8.7
	850	−3.0	−24.1	−29.0	−16.3	−10.9	−20.4	0.5	10.4	27.1	12.2	7.3	29.0
	875	−9.6	−27.8	−32.1	−21.6	−17.2	−25.6	2.0	14.1	36.6	19.9	14.2	47.8
	900	−18.3	−34.0	−38.0	−29.4	−25.9	−33.6	4.5	20.9	56.3	34.8	27.4	93.6
15 mm	825	17.7	−15.1	−21.8	−2.0	8.6	−6.5	−2.1	4.5	13.5	1.0	−3.6	5.5
	850	2.8	−21.6	−26.8	−13.4	−6.4	−18.1	−0.5	8.6	23.2	9.3	3.9	23.9
	875	−6.9	−27.0	−31.6	−21.1	−15.7	−25.7	1.4	13.4	35.4	19.0	12.5	48.2
	900	−24.8	−39.2	−42.8	−36.1	−32.7	−40.4	7.1	30.2	88.3	58.8	46.1	209.4

675/850, 675/875, 750/825, 760/825, 760/850, and 775/825 nm for $h_f<10$ mm. In addition to these pairs, $C_{\mathrm{HbO}_2\to\mathrm{Hb},3.0,h_f}^{\lambda_1,\lambda_2}$ had low crosstalk values also for pairs 675/900, and 700/825 nm. Higher crosstalk magnitudes where computed for the choice of a higher λ_2 for a fixed λ_1 at a given h_f.

Crosstalk values for a source-detector distance of $r=4.0$ cm results in slightly smaller values. At $h_f=0$, 5, 10, and 15 mm, $C_{\mathrm{HbO}_2\to\mathrm{Hb},4.0,h_f}$ was 9.0 ± 5.6, 11.5 ± 9.2, 19.3 ± 17.6, and $22.6\pm27.4\%$, and $C_{\mathrm{Hb}\to\mathrm{HbO}_2,4.0,h_f}$ was 14.1 ± 4.4, 15.3 ± 7.5, 20.1 ± 10.0, and $20.6\pm11.0\%$, respectively.

5 Discussion

We showed that the presence of a fat tissue layer causes underestimation error and crosstalk problems in cw-NIRS muscle measurements and that these problems are fat-thickness dependent. The main cause of these problems is the homogeneous medium assumption in the MBLL calculations with the use of a constant path length instead of fat thickness and wavelength-dependent mean partial path length in the muscle layer. The fat layer has a lower absorption coefficient than the underlying muscle layer and it has been shown[30,32,33,54] that as the fat layer thickens, probed volume by NIRS system also increases (the "banana" gets fatter). However, as the banana gets fatter, probed muscle volume decreases ($\langle L_m^\lambda \rangle$ decreases). Thicker fat layer leads to an increase in $\langle L^\lambda \rangle$ and $\langle L_f^\lambda \rangle$ and detected light intensity for the considered wavelengths in the 675 to 900-nm range, as shown in Sec. 4.1. Similar findings were reported in the literature such as the inverse relation between $\langle L_m \rangle$ and h_f found by simulation studies[25,30,31,34,35,54–56] and by theoretical investigations.[55] Higher detected light intensities have been also reported for thicker fat layer.[32,33,54,57]

There is also a strong wavelength dependency of $\langle L_m^\lambda \rangle$. The concentration of HbO_2 (taken as 70%) is higher than [Hb], and for longer wavelengths, $\epsilon_{\mathrm{HbO}_2}^\lambda$ is higher, which result in $\mu_{a,m}^\lambda$ increasing, leading to a decrease in $\langle L_m^\lambda \rangle$ and $\langle L^\lambda \rangle$ for longer wavelengths. In experimental studies, wavelength dependency has been reported[58–60] only for the DPF factor, since it is impossible to measure and isolate $\langle L_m^\lambda \rangle$ from a layered structure. Duncan et al.[61] reports DPF values of 4.43 ± 0.86 (5.78 ± 1.05) at 690 nm, and 3.94 ± 0.78 (5.33 ± 0.95) at 832 nm in the forearm (calf) for $r=4.5$ cm. In the same study, a significant female/male difference in the DPF values was shown, with values of 4.34 ± 0.78 for females and

3.53 ± 0.55 for males in the forearm at 832 nm. For $r > 2.5$ cm, DPF has been shown to be almost constant by van der Zee et al.,[60] where it was also stated that a female/male difference was present with mean DPF values of 5.14 ± 0.43 for females versus 3.98 ± 0.46 for males at 761 nm in the adult calf, but no difference was observed in the adult forearm (both DPF are 3.59 ± 0.32). A general trend of DPF decrease in 740- to 840-nm range was also found by Essenpreis et al.,[58] although no significant female/male difference was observed. In these studies, a female/male difference was attributed to fat/muscle ratio differences, although statistics concerning fat thicknesses were not present about the subjects in the studies.

In this study, we investigated the error in the estimation of the concentration changes using MBLL with homogeneous medium assumption under two headings: an underestimation error and crosstalk. We showed that fat thickness has a strong effect on both. The means of both absolute underestimation errors and absolute crosstalk over the considered wavelength pairs were calculated to be high for thick fat layer, as stated in Sec. 4.2 and 4.3. As stated, a decrease of $\langle L_m^\lambda \rangle$ with increased h_f and the use of a fixed DPF value in MBLL calculations because of the homogeneous medium assumption leads to rise in underestimation error. Crosstalk depends on $\langle L_m^\lambda \rangle$ but not the used DPF value when a wavelength-independent DPF is used. The wavelength dependency of $\epsilon_{HbO_2}^\lambda$ and ϵ_{Hb}^λ as well as the difference between them also affect crosstalk.

The choice of wavelength pair had a significant impact on the errors. The variability in the absolute underestimation errors for different wavelength pairs is higher for low fat thickness values while the variability in the absolute crosstalk for different wavelength pairs increases with increasing fat thickness. The means of absolute underestimation errors and absolute crosstalk were found to be higher for $E_{HbO_2,3.0,h_f}$ and $C_{Hb \to HbO_2,3.0,h_f}$. These findings are related to wavelength dependency of $\langle L_m^\lambda \rangle$ and specific absorption coefficients. Note $\langle L_m^\lambda \rangle$ has a decreasing trend at longer wavelengths and ϵ_{Hb}^λ ($\epsilon_{HbO_2}^\lambda$) is higher (lower) for wavelengths less than 798 nm, the isobestic point. In more detail, the reason for a higher underestimation error of $E_{HbO_2,3.0,h_f}$ with respect to $E_{Hb,3.0,h_f}$ can be explained by ΔOD^{λ_2} ($\propto \langle L_m^{\lambda_2} \rangle$) being more heavily weighted by the real concentration change of $\Delta[HbO_2]_m$ in the muscle layer than $\Delta[Hb]_m$. In the MBLL equations, measured ΔOD^λ's are assumed to be proportional to DPF $\times r$ instead of unavailable $\langle L_m^\lambda \rangle$. Wrongly used DPF $\times r$ overestimates the $\langle L_m^\lambda \rangle$ (leading to underestimation error for concentration change), however, the degree of path length overestimation is higher for longer wavelength since $\langle L_m^\lambda \rangle$ decreases with wavelength. Hence, the path length overestimation because of homogeneous medium assumption is higher for measured optical density change ΔOD^{λ_2} leading to more underestimation error for $\Delta[HbO_2]_{MBLL}$.

There is one previous study on crosstalk for muscle cw-NIRS measurements by Iwasaki and Okada.[42] This analysis was done for a fixed fat thickness of 4 mm, a two-wavelength system was assumed, λ_2 was fixed at 830 nm, and r was taken as 2.0 or 4.0 cm. The 720/830-nm and 780/830-nm pairs were found to be the favorable pair selections resulting in minimal crosstalk. In our study, the 775/825-nm pair also

gave low crosstalk values along with the 750/825- and 760/825-nm pairs, for both $C_{HbO_2 \to Hb}^{\lambda_1, \lambda_2}$ and $C_{Hb \to HbO_2}^{\lambda_1, \lambda_2}$. Iwasaki and Okada[42] found negative $C_{HbO_2 \to Hb}^{\lambda_1, \lambda_2}$ values and positive $C_{Hb \to HbO_2}^{\lambda_1, \lambda_2}$ values; however, we calculated not only opposite signs but also different magnitudes. These could be due to choice of muscle absorption coefficients, the values in this study range between 2.1 to 3.7 times higher than the values used in our study. We also looked at the effect of fat thickness variation on crosstalk and found a rise in the mean of absolute crosstalk values over the considered wavelength pairs for an increase in fat thickness. Moreover, other λ_2 values were studied, up to 900 nm. There was an increase in crosstalk amplitudes for an increase in λ_2 for values higher than 825 nm for a fixed λ_1 at a given h_f value. The absolute values of $C_{HbO_2 \to Hb,3.0}^{\lambda_1, \lambda_2}$ and $C_{Hb \to HbO_2,3.0}^{\lambda_1, \lambda_2}$ were calculated to be less than 11% for the 675/825, 675/850, 675/875-, 750/825-, 760/825-, 760/850-, and 775/825-nm pairs for $h_f < 10$ mm.

Arterial occlusion is employed in cw-NIRS measurements to estimate muscle oxygen consumption. In this case, ideally blood volume remains constant, while $\Delta[HbO_2]_m$ decreases and $\Delta[Hb]_m$ increases in equal magnitudes in the probed volume. Using Eq. (13), the estimation errors were found to be 10.6 ± 5.2, 30.7 ± 4.6, and $54.6 \pm 4.1\%$ for $\Delta[Hb]_{MBLL}$ and 15.1 ± 4.3, 34.3 ± 3.7, and $57.1 \pm 3.2\%$ for $\Delta[HbO_2]_{MBLL}$ at $h_f = 0$, 2, 4 mm respectively, computed over 24 wavelength pairs ($r = 3.0$ cm, DPF=4.37) These estimation errors for the two chromophores are closer compared to the differences between underestimation errors (Sec. 4.2) due to the crosstalk. The estimation error for $\Delta[Hb]_{MBLL}$ is higher than the underestimation error $E_{Hb,3.0,h_f}$, while estimation error of $\Delta[HbO_2]_{MBLL}$ is lower than the underestimation error $E_{HbO_2,3.0,h_f}$. For this protocol, the minimum estimation errors were found for the 700/825- and 725/825-nm pairs. For a fixed λ_2, the estimation errors for the occlusion protocol were found to be low for choice of 700 or 725 nm as λ_1, while for fixed λ_1, errors rise for an increase in λ_2, for both $\Delta[HbO_2]_{MBLL}$ and $\Delta[Hb]_{MBLL}$.

The error analysis in this study showed the clear failure of the homogenous medium assumption and the requirement to correct cw-NIRS measurements even for low fat thickness values, although it was stated that correction may not be required for less than 5 mm fat thickness by Yang et al.[57] There are already several proposed approaches for cw-NIRS measurement corrections, in particular for $m\dot{V}O_2$. Several investigators[25,32,55] have proposed correction algorithms using theoretically determined $\langle L_m \rangle$. Niwayama et al.[56,62,63] combined the results of simulations and experiments (for $\langle L_m \rangle$, detected light intensities, and experimental sensitivities) to obtain correction curves for $m\dot{V}O_2$. Utilizing these corrections, the variance of the experimental $m\dot{V}O_2$ results were reduced,[56,63] moreover, a higher correlation was found between $m\dot{V}O_2$ values measured by ^{31}P-NMR and corrected $m\dot{V}O_2$ values measured[62] by cw- NIRS. Yet another correction algorithm was proposed by the same group in which a relationship between detected light intensity and measurement sensitivity was utilized as an empirical technique to reduce
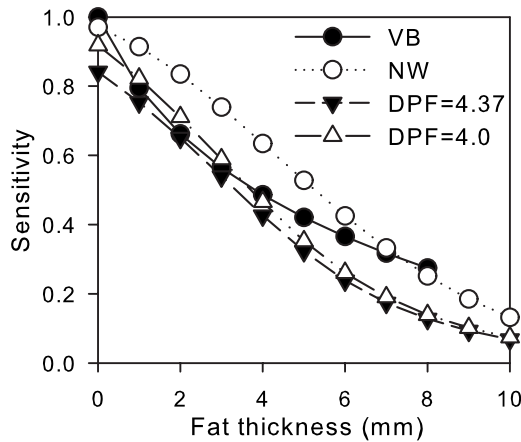
Fig. 4 Normalized oxygen consumption curve of van Beekvelt et al.[36] (denoted by VB), measurement correction curve of Niwayama et al.[63] (denoted by NW), computed $\Delta[HbO_2]_{MBLL}$ for ischemia protocol (for unit magnitude and opposite $\Delta[Hb]_m$ and $\Delta[HbO_2]_m$ changes, obtained for the 750/850-nm pair) using of DPF values of 4.37 (denoted by DPF=4.37) and 4.0 (denoted by DPF=4.0).

the variance in $m\dot{V}O_2$ findings due to fat thickness.[32,33,64] Yang et al.[57] proposed a correction for intensity of cw-NIRS measurements using a polynomial fit to detected intensity change with fat thickness. Lin et al.[65] used a neural-network-based algorithm for spatially resolved reflectance, first to find the optical coefficients of the top layer and then that of the layer below, assuming the top layer thickness is known. There are also broadband cw-NIRS techniques. One method orthogonalizes the spectra collected at a long source-detector distance (r) to the spectra collected at a short r and maps to the long r space.[66,67] Another one uses multiple detectors and the derivative of attenuation with respect to distance, utilizing a particular wavelength sensitive to fat thickness.[68,69]

Figure 4 shows four cw-NIRS measurement sensitivity curves. The first curve from our study is the calculated $\Delta[HbO_2]_{MBLL}$ computed for the ischemia protocol (for unit magnitude and opposite $\Delta[Hb]_m$ and $\Delta[HbO_2]_m$) using DPF=4.37, at a 750/850-nm pair (r=3.0 cm). The computed $\Delta[Hb]_{MBLL}$ for the same conditions (not shown) has a slightly higher sensitivity. The sensitivity curve of Niwayama et al.[63] is proposed for muscle measurement correction by dividing the calculated concentration changes by itself—given by $\exp[-((h_f+h_s)/8.0)^2]$, using the 760/840-nm pair for r=3.0 cm, we take h_s to be 1.4 mm. The curve of Niwayama et al.[63] indicates higher sensitivity than the one our curve predicts. For the computed $\Delta[HbO_2]_{MBLL}$, taking a lower DPF value of 4.0 (the value used in the Niwayama et al.[63]) leads to a higher sensitivity. Yet another curve is derived from the experimental resting state oxygen consumption curve of van Beekvelt et al.[36] [$m\dot{V}O_2$=0.18 to $-0.14 \times \log_{10}(hf+hs)$ ml of O_2 min^{-1} 100 g^{-1}, used DPF=4.0 cm, r=3.5 cm, three wavelengths a 770/850/905-nm system, we take h_s as 1.4 mm) by normalizing it to its value at a 0-mm fat thickness. The study had 78 volunteers with highest fat (plus skin) thickness of 8.9 mm (approximating a 7.5-mm fat thickness), hence shown up to h_f=8 mm. It is closer to our curve for low-fat-thickness values (<4 mm) but presents

higher sensitivity for higher fat thickness values and becomes closer to the curve of Niwayama et al.[63] van Beekvelt et al.[36] reports a 50% decrease in experimentally found oxygen consumption ($m\dot{V}O_2$) for fat thickness (including skin) in a range from 5 to 10 mm. Niwayama et al.[56,63] reports of a roughly 50% decrease in cw-NIRS measurement sensitivity for a two-fold increase in fat (including skin) thickness, but the range for fat thickness is not given. In our study, we calculated a nearly 55% decrease in the $\Delta[HbO_2]_{MBLL}$ and $\Delta[Hb]_{MBLL}$ for the ischemia protocol at 750/850 and 775/850 nm (the closest pairs to the wavelengths used in the mentioned studies) for h_f increase from 3 to 6 mm, while the decrease becomes nearly 34% for h_f=2 to 4 mm, and 70% for h_f=4 to 8 mm.

MBLL calculations are based on a linear approximation for the relationship of optical density change to absorption coefficient change, which leads to deviations for large concentration changes, as shown by Shao et al.[70] The presence of the fat layer deteriorates the linearity of measurement characteristics investigated by Lin et al.[25] In our study, we assumed small concentration changes. In quantitative studies aimed at oxygen consumption calculations, concentration change rates within small time scales during ischemia are typically used. In the experimental study of Ferrari et al.,[71] a difference of $\Delta[HbO_2] - \Delta[Hb]$ was computed for ischemia alone and for ischemia with maximal voluntary contraction. For these measurements, desaturation rates were computed with constant DPF and with changing DPF values found using time-resolved spectroscopy with the same experiment protocols. Similar rate values were calculated within short time scales.

The effect of fat layer thickness on cw-NIRS measurements is very explicit and dominant; note, however, that partial path length values, detected intensities, underestimation errors, and crosstalk are all subject to both intrasubject and intersubject variability because of optical coefficients' variability of tissue layers, variability in physiological status, muscle anatomy differences, and anisotropy in the skin[72] and in the muscle.[73]

An increase in the source-detector distance leads to lower errors because of increased $\langle L_m \rangle$, however, signal-to-noise ratio (SNR) also decreases since detected intensity decreases leading to a trade-off. It may be possible to discover an optimal source-detector distance based on optimization of SNR maximization and error minimization,[35,54] by also taking into account the fat thickness of the subject.

6 Conclusion

The fat layer influence on muscle cw-NIRS measurements based on MBLL calculations with homogeneous medium assumption was investigated for both underestimation error and crosstalk using Monte Carlo simulations for a two-wavelength system. Although the computed values of underestimation errors and crosstalk are dependent on the "true" optical coefficients of the tissue layers, and hence could change for each subject, an explicit finding is that the mean values of the absolute underestimation errors and absolute crosstalk computed over the considered wavelength pairs increase for the thicker of the fat layer. The means of absolute underestimation errors $E_{HbO_2,3.0,h_f}$ and absolute crosstalk $C_{Hb\to HbO_2,3.0,h_f}$ over the considered wavelength pairs were found to be higher,

while due to the crosstalk, the estimation errors for the concentration changes of the two chromophores were calculated to be closer for the ischemia protocol. These errors also depended on the wavelength pair selection for the two-wavelength system with greater impact on the crosstalk. This dependency of wavelength leads to the fact that correction algorithms should be dependent on the choice of wavelengths, although different wavelength combinations can have very similar sensitivities. The measurement of the fat thickness values and providing information about it should become a standard routine, as suggested by van Beekvelt et al.[74] for the cw-NIRS measurements.

Acknowledgments

References

1. M. Cope, "The application of near infrared spectroscopy to non invasive monitoring of cerebral oxygenation in the newborn infant," PhD Thesis, University College London (1991).
2. E. Gratton, V. Toronov, U. Wolf, M. Wolf, and A. Webb, "Measurement of brain activity by near-infrared light," *J. Biomed. Opt.* **10**(1), 11008 (2005).
3. A. Villringer and B. Chance, "Non-invasive optical spectroscopy and imaging of human brain function," *Trends Neurosci.* **20**, 435–442 (1997).
4. E. Heffer, V. Pera, O. Schutz, H. Siebold, and S. Fantini, "Near-infrared imaging of the human breast: complementing hemoglobin concentration maps with oxygenation images," *J. Biomed. Opt.* **9**(6), 1152–1160 (2004).
5. M. Ferrari, T. Binzoni, and V. Quaresima, "Oxidative metabolism in muscle," *Philos. Trans. R. Soc. London, Ser. B* **352**, 677–683 (1997).
6. V. Quaresima, R. Lepanto, and M. Ferrari, "The use of near infrared spectroscopy in sports medicine," *J. Sports Med. Phys. Fitness* **43**, 1–13 (2003).
7. T. Hamaoka, K. K. McCully, V. Quaresima, K. Yamamoto, and B. Chanceh, "Near-infrared spectroscopy/imaging for monitoring muscle oxygenation and oxidative metabolism in healthy and diseased humans," *J. Biomed. Opt.* **12**(6), 062105 (2007).
8. S. Suzuki, S. Takasaki, T. Ozaki, and Y. Kobayashi, "Tissue oxygenation monitor using NIR spatially resolved spectroscopy," in *Optical Tomography and Spectroscopy of Tissue III*, B. Chance, R. R. Alfano, and B. J. Tromberg, Eds., *Proc. SPIE* **3597**, 582–592, (1999).
9. D. T. Delpy, M. Cope, P. van der Zee, S. Arridge, S. Wray, and J. Wyatt, "Estimation of optical pathlength through tissue from direct time of flight measurement," *Phys. Med. Biol.* **33**, 1433–1442 (1988).
10. S. R. Arridge, M. Cope, and D. T. Delpy, "The theoretical basis for the determination of optical pathlengths in tissue: temporal and frequency analysis," *Phys. Med. Biol.* **37**, 1531–1560 (1992).
11. A. Kienle and T. Glanzmann, "In vivo determination of the optical properties of muscle with time-resolved reflectance using a layered model," *Phys. Med. Biol.* **44**(11), 2689–2702 (1999).
12. R. J. Hunter, M. S. Patterson, T. J. Farrell, and J. E. Hayward, "Haemoglobin oxygenation of a two-layer tissue-simulating phantom from time-resolved reflectance: effect of top layer thickness," *Phys. Med. Biol.* **47**(2), 193–208 (2002).
13. A. Kienle, M. S. Patterson, N. Dögnitz, R. Bays, G. Wagnivres, and H. van den Bergh, "Noninvasive determination of the optical properties of two-layered turbid media," *Appl. Opt.* **37**(4), 779–791 (1998).
14. F. Fabbri, A. Sassaroli, M. E. Henry, and S. Fantini, "Optical measurements of absorption changes in two-layered diffusive media," *Phys. Med. Biol.* **49**, 1183–1201 (2004).
15. A. Li, R. Kwong, A. Cerussi, S. Merritt, C. Hayakawa, and B. Tromberg, "Method for recovering quantitative broadband diffuse optical spectra from layered media," *Appl. Opt.* **46**(21), 4828–4833 (2007).
16. J. Ripoll, V. Ntziachristos, J. P. Culver, D. N. Pattanayak, A. G. Yodh, and M. Nieto-Vesperinas, "Recovery of optical parameters in multiple-layered diffusive media: theory and experiments," *J. Opt. Soc. Am. A* **18**(4), 821–830 (2001).
17. F. Martelli, S. D. Bianco, G. Zaccanti, A. Pifferi, A. Torricelli, A. Bassi, P. Taroni, and R. Cubeddu, "Phantom validation and in vivo application of an inversion procedure for retrieving the optical properties of diffusive layered media from time-resolved reflectance measurements," *Opt. Lett.* **29**, 2037–2039 (2004).
18. F. Martelli, A. Sassaroli, S. D. Bianco, and G. Zaccanti, "Solution of the time-dependent diffusion equation for a three-layer medium: application to study photon migration through a simplified adult head model," *Phys. Med. Biol.* **52**, 2827–2843 (2007).
19. C. Sato, M. Shimada, Y. Yamada, and Y. Hoshi, "Extraction of depth-dependent signals from time-resolved reflectance in layered turbid media," *J. Biomed. Opt.* **10**(6), 064008 (2005).
20. J. Steinbrink, H. Wabnitz, H. Obrig, A. Villringer, and H. Rinneberg, "Determining changes in NIR absorption using a layered model of the human head," *Phys. Med. Biol.* **46**(3), 879–896 (2001).
21. E. Okada, M. Firbank, and D. T. Delpy, "The effect of overlying tissue on the spatial sensitivity profile of near-infrared spectroscopy," *Phys. Med. Biol.* **40**(12), 2093–2108 (1995).
22. M. Hiraoka, M. Firbank, M. Essenpreis, M. Cope, S. R. Arridge, P. van der Zee, and D. T. Delpy, "A Monte Carlo investigation of optical pathlength in inhomogeneous tissue and its application to near-infrared spectroscopy," *Phys. Med. Biol.* **38**(12), 1859–1876 (1993).
23. D. A. Boas, T. Gaudette, G. Strangman, X. Cheng, J. J. Marota, and J. B. Mandeville, "The accuracy of near infrared spectroscopy and imaging during focal changes in cerebral hemodynamics," *Neuroimage* **13**, 76–90 (2001).
24. G. Strangman, M. A. Franceschini, and D. A. Boas, "Factors affecting the accuracy of near-infrared spectroscopy concentration calculations for focal changes in oxygenation parameters," *Neuroimage* **18**, 865–879 (2003).
25. L. Lin, M. Niwayama, T. Shiga, N. Kudo, M. Takahashi, and K. Yamamoto, "Influence of a fat layer on muscle oxygenation measurement using near-IR spectroscopy: quantitative analysis based on two-layered phantom experiments and Monte Carlo simulation," *Front Med. Biol. Eng.* **10**(1), 43–58 (2000).
26. T. J. Farrell, M. S. Patterson, and M. Essenpreis, "Influence of layered tissue architecture on estimates of tissue optical properties obtained from spatially resolved diffuse reflectometry," *Appl. Opt.* **37**(10), 1958–1972 (1998).
27. E. Okada and D. T. Delpy, "Near-infrared light propagation in an adult head model. ii. Effect of superficial tissue thickness on the sensitivity of the near-infrared spectroscopy signal," *Appl. Opt.* **42**(16), 2915–2922 (2003).
28. M. A. Franceschini, S. Fantini, L. A. Paunescu, J. S. Maier, and E. Gratton, "Influence of a superficial layer in the quantitative spectroscopic study of strongly scattering media," *Appl. Opt.* **37**(31), 7447–7458 (1998).
29. S. Homma, T. Fukunaga, and A. Kagaya, "Influence of adipose tissue thickness on near infrared spectroscopic signal in the measurement of human muscle," *J. Biomed. Opt.* **1**, 418–424 (1996).
30. K. Matsushita, S. Homma, and E. Okada, "Influence of adipose tissue on muscle oxygenation measurement with an NIRS instrument," *Proc. SPIE* **3194**, 159–165 (1998).
31. K. Matsushita and E. Okada, "Influence of adipose tissue on near infrared oxygenation monitoring in muscle," in *Proc. 20th Ann. Int. Conf. IEEE/EMBS (Hong Kong)*, Vol. **4**, pp. 1864–1867 (1998).
32. K. Yamamoto, M. Niwayama, L. Lin, T. Shiga, N. Kudo, and M. Takahashi, "Accurate NIRS measurement of muscle oxygenation by correcting the influence of a subcutaneous fat layer," *Proc. SPIE* **3194**, 166–173 (1998).
33. K. Yamamoto, M. Niwayama, L. Lin, T. Shiga, N. Kudo, and M. Takahashi, "Near-infrared muscle oximeter that can correct the influence of a subcutaneous fat layer," *Proc. SPIE* **3257**, 146–155 (1998).
34. L. Lin, M. Niwayama, T. Shiga, N. Kudo, M. Takahashi, and K. Yamamoto, "Two-layered phantom experiments for characterizing the influence of a fat layer on measurement of muscle oxygenation using nirs," *Proc. SPIE* **3257**, 156–166 (1998).
35. W. Feng, D. Haishu, T. Fenghua, Z. Jun, X. Qing, and T. Xianwu, "Influence of overlying tissue and probe geometry on the sensitivity of a near-infrared tissue oximeter," *Physiol. Meas* **22**(1), 201–208 (2001).

36. M. C. van Beekvelt, M. S. Borghuis, B. G. van Engelen, R. A. Wevers, and W. N. Colier, "Adipose tissue thickness affects in vivo quantitative near-IR spectroscopy in human skeletal muscle," *Clin. Sci. (Lond.)* **101**, 21–28 (2001).

37. E. Okada, M. Firbank, M. Schweiger, S. R. Arridge, M. Cope, and D. T. Delpy, "Theoretical and experimental investigation of near-infrared light propagation in a model of the adult head," *Appl. Opt.* **36**(1), 21–31 (1997).

38. M. Kohl, C. Nolte, H. R. Heekeren, S. Horst, U. Scholz, H. Obrig, and A. Villringer, "Determination of the wavelength dependence of the differential pathlength factor from near-infrared pulse signals," *Phys. Med. Biol.* **43**(6), 1771–1782 (1998).

39. J. Mayhew, Y. Zheng, Y. Hou, B. Vuksanovic, J. Berwick, S. Askew, and P. Coffey, "Spectroscopic analysis of changes in remitted illumination: the response to increased neural activity in brain," *Neuroimage* **10**, 304–326 (1999).

40. K. Uludag, M. Kohl, J. Steinbrink, H. Obrig, and A. Villringer, "Cross talk in the Lambert-Beer calculation for near-infrared wavelengths estimated by Monte Carlo simulations," *J. Biomed. Opt.* **7**, 51–59 (2002).

41. M. Kohl, U. Lindauer, G. Royl, M. Kuhl, L. Gold, A. Villringer, and U. Dirnagl, "Physical model for the spectroscopic analysis of cortical intrinsic optical signals," *Phys. Med. Biol.* **45**(12), 3749–3764 (2000).

42. A. Iwasaki and E. Okada, "Influence of cross talk on near-infrared oxygenation monitoring of muscle," in *Proc. APBP 2004*, pp. 159–160 (2004).

43. A. Sassaroli and S. Fantini, "Comment on the modified Beer-Lambert law for scattering media," *Phys. Med. Biol.* **49**, N255–N257 (2004).

44. L. Kocsis, P. Herman, and A. Eke, "The modified Beer-Lambert law revisited," *Phys. Med. Biol.* **51**, N91–N98 (2006).

45. M. Sassaroli and D. L. Rousseau, "Time dependence of near-infrared spectra of photodissociated hemoglobin and myoglobin," *Biochemistry* **26**(11), 3092–3098 (1987).

46. N. Okui and E. Okada, "Wavelength dependence of crosstalk in dual-wavelength measurement of oxy- and deoxy-hemoglobin," *J. Biomed. Opt.* **10**(1), 11015 (2005).

47. C. R. Simpson, M. Kohl, M. Essenpreis, and M. Cope, "Near-infrared optical properties of ex vivo human skin and subcutaneous tissues measured using the Monte Carlo inversion technique," *Phys. Med. Biol.* **43**(9), 2465–2478 (1998).

48. F. A. Duck, *Physical Properties of Tissue: A Comprehensive Reference Book*, Academic Press, London (1990).

49. T. Hamaoka, T. Katsumura, N. Murase, S. Nishio, T. Osada, T. Sako, H. Higuchi, Y. Kurosawa, T. Shimomitsu, M. Miwa, and B. Chance, "Quantification of ischemic muscle deoxygenation by near infrared time-resolved spectroscopy," *J. Biomed. Opt.* **5**, 102–105 (2000).

50. V. S. Hollis, "Non-invasive monitoring of brain tissue temperature by near-infrared spectroscopy," PhD thesis, University College London (2002).

51. L. Wang, S. L. Jacques, and L. Zheng, "MCML–Monte Carlo modeling of light transport in multi-layered tissues," *Comput. Methods Programs Biomed.* **47**, 131–146 (1995).

52. M. S. Patterson, B. C. Wilson, and D. R. Wyman, "The propagation of optical radiation in tissue ii. Optical properties of tissue and resulting fluence distributions," *Lasers Med. Sci.* **6**, 379–390 (1991).

53. F. P. Bolin, L. E. Preuss, R. C. Taylor, and R. J. Ference, "Refractive index of some mammalian tissues using a fiber optic cladding method," *Appl. Opt.* **28**(12), 2297–2303 (1989).

54. H. Ding, F. Wang, F. Lin, G. Wang, W. Li, and W. Lichty, "Analysis of the sensitivity of reflectance near-infrared tissue oximeter using the methods of simulation and experiment," *Proc. SPIE* **3863**, 59–65 (1999).

55. A. Kienle, M. S. Patterson, N. Doegnitz-Utke, R. Bays, G. A. Wagnieres, and H. van den Bergh, "Two-layered turbid media with steady-state and frequency- and time-domain reflectance," *Proc. SPIE* **3194**, 269–278 (1998).

56. M. Niwayama, L. Lin, J. Shao, T. Shiga, N. Kudo, and K. Yamamoto, "Quantitative measurement of muscle oxygenation by NIRS: analysis of the influences of a subcutaneous fat layer and skin," *Proc. SPIE* **3597**, 291–299 (1999).

57. Y. Yang, O. Soyemi, M. Landry, and B. Soller, "Influence of a fat layer on the near infrared spectra of human muscle: quantitative analysis based on two-layered Monte Carlo simulations and phantom experiments," *Opt. Express* **13**(5), 1570–1579 (2005).

58. M. Essenpreis, M. Cope, C. E. Elwell, S. R. Arridge, P. van der Zee, and D. T. Delpy, "Wavelength dependence of the differential pathlength factor and the log slope in time-resolved tissue spectroscopy," *Adv. Exp. Med. Biol.* **333**, 9–20 (1993).

59. A. Duncan, T. L. Whitlock, M. Cope, and D. T. Delpy, "Measurement of changes in optical pathlength through human muscle during cuff occlusion on the arm," *Opt. Laser Technol.* **27**(4), 269–274 (1995).

60. P. van der Zee, M. Cope, S. R. Arridge, M. Essenpreis, L. A. Potter, A. D. Edwards, J. S. Wyatt, D. C. McCormick, S. C. Roth, and E. O. Reynolds, "Experimentally measured optical pathlengths for the adult head, calf and forearm and the head of the newborn infant as a function of inter optode spacing," *Adv. Exp. Med. Biol.* **316**, 143–153 (1992).

61. A. Duncan, J. H. Meek, M. Clemence, C. E. Elwell, L. Tyszczuk, M. Cope, and D. T. Delpy, "Optical pathlength measurements on adult head, calf and forearm and the head of the newborn infant using phase resolved optical spectroscopy," *Phys. Med. Biol.* **40**, 295–304 (1995).

62. M. Niwayama, T. Hamaoka, L. Lin, J. Shao, N. Kudo, C. Katoh, and K. Yamamoto, "Quantitative muscle oxygenation measurement using NIRS with correction for the influence of a fat layer: comparison of oxygen consumption rates with measurements by other techniques," *Proc. SPIE* **3911**, 256–265 (2000).

63. M. Niwayama, L. Lin, J. Shao, N. Kudo, and K. Yamamoto, "Quantitative measurement of muscle hemoglobin oxygenation using near-infrared spectroscopy with correction for the influence of a subcutaneous fat layer," *Rev. Sci. Instrum.* **71**(12), 4571–4575 (2000).

64. M. Niwayama, T. Shiga, L. Lin, N. Kudo, M. Takahashi, and K. Yamamoto, "Correction of the influences of a subcutaneous fat layer and skin in a near-infrared muscle oximeter," in *Proc. 20th Ann. Int. Conf. IEEE/EMBS (Hong Kong)*, Vol. **4**, pp. 1849–1850 (1998).

65. L. Lin, Y. Chen, G. Li, J. Gao, and K. Wu, "A novel method for determination of the optical properties of two-layer tissue model from spatially resolved diffuse reflectance," in *Optics in Health Care and Biomedical Optics: Diagnostics and Treatment II*, B. Chance, M. Chen, A. E. T. Chiou, and Q. Luo, Eds., *Proc. SPIE* **5630**, 486–497 (2005).

66. Y. Yang, M. R. Landry, O. O. Soyemi, M. A. Shear, D. S. Anunciacion, and B. R. Soller, "Simultaneous correction of the influence of skin color and fat on tissue spectroscopy by use of a two-distance fiber-optic probe and orthogonalization technique," *Opt. Lett.* **30**(17), 2269–2271 (2005).

67. Y. Yang, O. Soyemi, P. J. Scott, M. R. Landry, S. M. Lee, L. Stroud, and B. R. Soller, "Quantitative measurement of muscle oxygen saturation without influence from skin and fat using continuous-wave near infrared spectroscopy," *Opt. Express* **15**(21), 13715–13730 (2007).

68. D. Geraskin, P. Platen, J. Franke, and M. Kohl-Bareis, in "Algorithms for muscle oxygenation monitoring corrected for adipose tissue thickness," in *Diffuse Optical Imaging of Tissue*, *Proc. SPIE* **6629**, 66290P (2007).

69. D. Geraskin, P. Platen, J. Franke, and M. Kohl-Bareis, "Algorithms for Muscle Oxygenation Monitoring Corrected for Adipose Tissue Thickness," in *Advances in Medical Engineering*, **114**, pp. 384–388, Springer (2007).

70. J. Shao, L. Lin, M. Niwayama, N. Kudo, and K. Yamamoto, "Determination of a quantitative algorithm for the measurement of muscle oxygenation using cw near-infrared spectroscopy: mean optical pathlength without the influence of the adipose tissue," *Proc. SPIE* **4082**, 76–86 (2000).

71. M. Ferrari, Q. Wei, R. A. D. Blasi, V. Quaresima, and G. Zaccanti, "Variability of human brain and muscle optical pathlength in different experimental conditions," in *Photon Migration and Imaging in Random Media and Tissues*, *Proc. SPIE* **1888**, 466–472 (1993).

72. S. Nickell, M. Hermann, M. Essenpreis, T. J. Farrell, U. Krämer, and M. S. Patterson, "Anisotropy of light propagation in human skin," *Phys. Med. Biol.* **45**, 2873–2886 (2000).

73. T. Binzoni, C. Courvoisier, R. Giust, G. Tribillon, T. Gharbi, J. C. Hebden, T. S. Leung, J. Roux, and D. T. Delpy, "Anisotropic photon migration in human skeletal muscle," *Phys. Med. Biol.* **51**, N79–N90 (2006).

74. M. C. P. van Beekvelt, B. G. M. van Engelen, R. A. Wevers, and W. N. J. M. Colier, "Near-infrared spectroscopy in chronic progressive external ophthalmoplegia: Adipose tissue thickness confounds decreased muscle oxygen consumption," *Ann. Neurol.* **51**(2), 272–273 (2002).